

Edge states of a Bi_2Se_3 nanosheet in a perpendicular magnetic field

S.P.J. Koenis,* L. Maisel Licerán, and H.T.C. Stoof

*Institute for Theoretical Physics and Center for Extreme Matter and Emergent Phenomena
Utrecht University, Princetonplein 5, 3584 CC Utrecht, The Netherlands*

(Dated: December 12, 2025)

Conventional wisdom dictates that the conducting edge states of two-dimensional topological insulators of the Bi_2Se_3 family are protected by time-reversal symmetry. However, theoretical bulk calculations and a recent experiment show that the edge states persist in the presence of large external magnetic fields. To address this apparent contradiction, we have developed an analytical description for the edge-state wave function of a semi-infinite sample in a perpendicular magnetic field. Our description relies on the usual bulk Landau levels, together with additional states arising due to the presence of the hard wall, which are unnormalizable in the infinite system. The analytical wave functions agree extremely well with numerical calculations and can be used to directly analyze the behavior of the edge states in a magnetic field.

I. INTRODUCTION

In recent years, interest in topological insulators (TIs) has surged due to the prospects of energy-efficient electronics and transport applications [1–5]. These systems have gapped bulk states and gapless edge or surface modes, where the latter are topologically protected against disorder scattering. A well-known example of this phenomenon is the quantum spin-Hall effect (QSHE), where two helical modes travel in opposite directions along the boundary of the system [6].

An example of such TIs is bismuth selenide (Bi_2Se_3), a three-dimensional (3D) TI consisting of quintuple layers stacked on top of each other and bound by van der Waals forces. It has attracted particularly significant attention due to its large band gap of 0.3 eV and its promising applicability [7–10]. Its topological properties arise from the spin-orbit coupling around the Γ point [11, 12], which gives rise to topologically protected Dirac states at the top and bottom surfaces of thick samples. Furthermore, in samples of less than six quintuple layers in thickness, the upper and lower surface modes couple via quantum tunneling and a thickness-dependent energy gap opens up [13]. For some thicknesses the gap is topological, causing a one-dimensional edge (1D) state to appear at the boundaries of the two-dimensional (2D) sample [14–16]. These edge states have been studied in more detail theoretically [17, 18] and also experimentally via angle-resolved photoemission spectroscopy [19, 20] and scanning tunnelling microscopy (STM) [21]. The tunability of this energy gap makes these thin film TIs desirable for electronic device applications. With these applications in mind, it is important to characterize and understand their edge states not only under ideal circumstances, but also in the presence of external perturbations.

It is often stated that the edge states of a TI such as Bi_2Se_3 are protected by time-reversal symmetry [22–24]. However, a recent experiment shows with STM measurements that the edge states in Bi_2Se_3 nanosheets can exist when this symmetry is broken by a perpendicular magnetic field of up to at least 5 T [25]. Theoretical calculations for the infinite Bernevig–

Hughes–Zhang (BHZ) model for the QSHE have found evidence that the edge state can persist up to high magnetic fields [24]. These calculations rely on the bulk-boundary correspondence to draw conclusions about the edge states [26], but the latter are not computed explicitly. Indeed, an analytic calculation of the edge states to investigate their behaviour under a magnetic field has, to the best of our knowledge, not been performed. The goal of this article is thus to provide a general description of the edge states of a Bi_2Se_3 nanosheet in a perpendicular magnetic field. This sheds further light on the robustness of the edge state in the absence of time-reversal symmetry and lays the groundwork for future effective-model calculations.

Our article is structured as follows. In Sec. II we outline the derivation of the Hamiltonian for a thin Bi_2Se_3 nanosheet, and its solution in the infinite volume case. In Sec. III we investigate the edge state of the Bi_2Se_3 nanosheet by introducing a hard wall in the system, effectively considering solutions in a semi-infinite nanosheet, and propose a basis of wave functions for analytically describing the 1D edge state at the boundary. Furthermore, we provide a step-by-step guide on how to find the analytical expression for the 1D edge mode traveling along the edge, yielding a dispersion relation of this edge state. In Sec. IV we compare this dispersion relation to numerical calculations. Finally, in Sec. V we summarize the findings of this article, and discuss potential avenues for further research.

II. BULK HAMILTONIAN

For the characterization of the edge states of Bi_2Se_3 , it will be useful to first take a close look at the bulk states in a nanosheet of this material. In this section we consider an infinite nanosheet of thickness L_z lying parallel to the xy plane. The Hamiltonian for such a system can be derived from the 3D $\mathbf{k} \cdot \mathbf{p}$ Hamiltonian for Bi_2Se_3 as explained in Refs. [18, 27], but we briefly outline the procedure here for completeness.

The starting point is the 3D Hamiltonian of the bulk material around the Γ -point, which for Bi_2Se_3 is given by the $\mathbf{k} \cdot \mathbf{p}$ model

* s.p.j.koenis@uu.nl

[28]

$$H(\mathbf{k}, k_z) = \epsilon(\mathbf{k}) \mathbb{I}_4 + \begin{bmatrix} \mathcal{M}(\mathbf{k}) & A_1 k_z & 0 & A_2 k_- \\ A_1 k_z & -\mathcal{M}(\mathbf{k}) & A_2 k_- & 0 \\ 0 & A_2 k_+ & \mathcal{M}(\mathbf{k}) & -A_1 k_z \\ A_2 k_+ & 0 & -A_1 k_z & -\mathcal{M}(\mathbf{k}) \end{bmatrix}. \quad (1)$$

Here, $\mathbf{k} \equiv (k_x, k_y)$, $k_{\pm} \equiv k_x \pm ik_y$, $\epsilon(\mathbf{k}) = C - D_1 k_z^2 - D_2(k_x^2 + k_y^2)$, $\mathcal{M}(\mathbf{k}) = M - B_1 k_z^2 - B_2(k_x^2 + k_y^2)$, and \mathbb{I}_4 the 4×4 identity matrix. The values of the parameters are taken from Ref. [23]. This Hamiltonian is expressed in the basis $\{|Bi^+, \uparrow\rangle, |Se^-, \uparrow\rangle, |Bi^+, \downarrow\rangle, |Se^-, \downarrow\rangle\}$, indexed by the orbitals closest to the Fermi surface and the spin of the electrons.

The effective Hamiltonian for an infinite nanosheet is obtained by restricting the size in the z direction from $-L_z/2$ to $L_z/2$, thereby breaking the translational symmetry in this direction. Hence, k_z ceases to be a good quantum number, and we must make the substitution $k_z \rightarrow -i\partial_z$. This yields a Hamiltonian which can be solved at the 2D Γ point $k_x = k_y = 0$. The four states closest to the Fermi level are denoted by $\{\Phi_1(z), \Phi_2(z), \Phi_3(z), \Phi_4(z)\}$ and their analytical expressions can be found in Ref. [29]. We can obtain a low-energy effective model by projecting the Hamiltonian $H(\mathbf{k}, -i\partial_z)$ onto the subspace spanned by these four solutions, i.e.,

$$H_{\text{eff}}(\mathbf{k})_{\alpha\beta} = \int_{-L_z/2}^{L_z/2} dz \Phi_{\alpha}^{\dagger}(z) H(\mathbf{k}, -i\partial_z) \Phi_{\beta}(z). \quad (2)$$

After a basis reordering the Hamiltonian decouples into the block-diagonal form $H_{\text{eff}} = \text{diag}(h'_+, h'_-)$, similar to the BHZ model, with

$$h'_{\tau_z}(\mathbf{k}) = E_0 - Dk^2 + v_F(k_y\sigma_x - k_x\sigma_y) + \tau_z \left(\frac{\Delta}{2} - Bk^2 \right) \sigma_z. \quad (3)$$

Here, v_F is the Fermi velocity, Δ the (inverted) band gap energy at the Γ point, σ_i the Pauli matrices, and $\tau_z = \pm 1$ the so-called hyperbola index. Note that the Pauli-matrices are not the direct physical spin operators, as is explained in Ref. [15]. In this article, we will drop the irrelevant constant term E_0 from Eq. (3), and use units such that $\hbar = 1$.

Next, we introduce a magnetic field in the z direction, $\mathbf{B} = \mathcal{B}\hat{z}$. This adds a Zeeman term depending on the effective magnetic moment μ_{eff} , and forces the replacement

$\hat{p}_i \rightarrow \hat{p}_i + eA_i$, with \mathbf{A} the magnetic vector potential and $e > 0$ the elementary charge. We will later see that a convenient choice for the vector potential is $(0, \mathcal{B}x, 0)$, so that k_y remains well defined. This yields the Hamiltonian which will be used throughout the rest of this article, namely

$$h_{\tau_z} = -De\mathcal{B}(\xi^2 - \partial_{\xi}^2)\mathbb{I}_2 + v_F\sqrt{e\mathcal{B}}(\xi\sigma_x - i\partial_{\xi}\sigma_y) + \tau_z \left(\frac{\Delta}{2} - Be\mathcal{B}(\xi^2 - \partial_{\xi}^2) \right) \sigma_z - \mu_{\text{eff}}\mathcal{B}\sigma_z. \quad (4)$$

For convenience, we have expressed everything in terms of the shifted position $\tilde{x} \equiv x + k_y l_{\mathcal{B}}^2$ and introduced the dimensionless parameter $\xi \equiv \tilde{x}/l_{\mathcal{B}}$, with $l_{\mathcal{B}} = 1/\sqrt{e\mathcal{B}}$ the magnetic length.

For all figures and explicit calculations in this paper we have taken $\Delta = 0.07$ eV, $D = -0.08$ eVnm² and $B = 0.1$ eVnm², which are not the values arising directly of the projection but most correctly reproduce the dispersion around the Γ point when only four states are considered [15]. We take $\mu_{\text{eff}} = g\mu_B$, with μ_B the Bohr magneton and g the electronic g factor whose value we take as 2 for simplicity and lack of experiments.

Note that h_{τ_z} is invariant under the simultaneous transformations $\tau_z \rightarrow -\tau_z$, $\mathcal{B} \rightarrow -\mathcal{B}$, and $k_y \rightarrow -k_y$, together with a reordering of the basis that switches the spins. Hence, without loss of generality, we assume that $\mathcal{B} > 0$ in the rest of the article.

A. Bulk Solution with $\mathcal{B} \neq 0$

We will now solve the eigenvalue equation arising from Eq. (4) to characterize the bulk solutions of this system. This has been done in Ref. [24], but we outline the calculation here as it will be useful for Sec. III. The problem is equivalent to a system of two coupled harmonic oscillators and can be solved analytically by introducing the operators

$$\hat{a}^{\dagger} = \frac{1}{\sqrt{2}}(\xi - \partial_{\xi}), \quad (5a)$$

$$\hat{a} = \frac{1}{\sqrt{2}}(\xi + \partial_{\xi}), \quad (5b)$$

where we call \hat{a}^{\dagger} the creation or raising operator and \hat{a} the annihilation or lowering operator. Using these, the Hamiltonian h_{τ_z} is rewritten as

$$h_{\tau_z} = \left[\tau_z \frac{\Delta}{2} - \mu_{\text{eff}}\mathcal{B} - 2\sqrt{e\mathcal{B}}(D + \tau_z B)(\hat{a}^{\dagger}\hat{a} + \frac{1}{2}) - v_F\sqrt{2e\mathcal{B}}\hat{a}^{\dagger} \right. \\ \left. - \tau_z \frac{\Delta}{2} + \mu_{\text{eff}}\mathcal{B} - 2\sqrt{e\mathcal{B}}(D - \tau_z B)(\hat{a}^{\dagger}\hat{a} + \frac{1}{2}) \right]. \quad (6)$$

Each diagonal term depends on $\hat{a}^{\dagger}\hat{a} + \frac{1}{2}$ and hence corresponds to a regular harmonic oscillator. The eigenfunctions of this term alone are the normalized Hermite functions [30]

$$\phi_n(x, k_y) = \frac{1}{\sqrt{2^n n! l_{\mathcal{B}} \sqrt{\pi}}} H_n(\xi) e^{-\xi^2/2}, \quad (7)$$

with $H_n(\xi)$ the Hermite polynomial of order n in terms of ξ . Eq. (7) gives the eigenfunctions of the diagonal part of the Hamiltonian of Eq. (6), and the eigenfunctions to the full

Hamiltonian can be constructed via the Ansatz

$$\begin{aligned}\psi_{\tau_z n, \text{bulk}}^{\pm}(x, k_y) &= \begin{bmatrix} \alpha_{\tau_z n}^{\pm} \phi_{n-1}(x, k_y) \\ \beta_{\tau_z n}^{\pm} \phi_n(x, k_y) \end{bmatrix} \\ &= \frac{1}{\sqrt{2^n n! l_B \sqrt{\pi}}} e^{-\xi^2/2} \begin{bmatrix} \sqrt{2n} \alpha_{\tau_z n}^{\pm} H_{n-1}(\xi) \\ \beta_{\tau_z n}^{\pm} H_n(\xi) \end{bmatrix}\end{aligned}\quad (8)$$

for some pair of numbers $v_{\tau_z n}^{\pm} = [\alpha_{\tau_z n}^{\pm}, \beta_{\tau_z n}^{\pm}]^T$ with $n \geq 1$. We call wave functions of this form the Landau states (LSs). The superscript \pm will represent two possible inequivalent solutions for a given τ_z and n . Letting the Hamiltonian act on this Ansatz and solving for nontrivial $v_{\tau_z n}^{\pm}$ yields the Landau levels (LLs) of the system, which read

$$E_{\tau_z n}^{\pm} = -2e\mathcal{B}Dn + e\mathcal{B}B\tau_z \pm \frac{1}{2}\sqrt{\mathcal{A}_{\tau_z n}}, \quad (9)$$

with

$$\mathcal{A}_{\tau_z n} = \left(2e\mathcal{B}(D - Bn\tau_z) - 2\mu_{\text{eff}}\mathcal{B} + \Delta\tau_z\right)^2 + 8e\mathcal{B}n\mathcal{V}_F^2. \quad (10)$$

The corresponding (unnormalized) eigenstate coefficients are

$$v_{\tau_z n}^{\pm} = \frac{\left[\Delta\tau_z + 2e\mathcal{B}(D - 2Bn\tau_z) - 2\mu\mathcal{B} \pm \sqrt{\mathcal{A}_{\tau_z n}}\right]}{2\mathcal{V}_F\sqrt{2e\mathcal{B}n}}. \quad (11)$$

We then have an infinite set of states with $n \geq 1$. Importantly, however, there is one additional solution for each τ_z , namely $n = 0$, with energy $E_{+1,0}^-(E_{-1,0}^+)$ for $\tau_z = +1$ ($\tau_z = -1$). Notice that in this case the superscript is fully determined by the sign of τ_z , and as such, we will drop it in the rest of this article for $n = 0$. The wave functions in both cases read $\psi_{0, \text{bulk}}(x, k_y) = [0, \phi_0(x, k_y)]^T$, and hence $v_{\tau_z n} = [0, 1]^T$. The energy levels of the bulk states for $\tau_z = +1$ correspond to the dashed lines of Fig. 1.

III. EDGE PHYSICS

We now turn to the primary focus of this article: the edge state of the Bi_2Se_3 nanosheets in a magnetic field. We introduce the edge state by considering a semi-infinite Bi_2Se_3 nanosheet of thickness L_z lying parallel to the xy plane as in the last section, but now only in the region $x \geq 0$. The edge states are localized close to the boundary at $x = 0$ and their momentum k_y along the y axis is a good quantum number. We assume a hard-wall boundary condition at $x = 0$. We choose $\mathbf{A} = (0, \mathcal{B}x, 0)$, so that the translational symmetry is only broken in the direction perpendicular to the edge and thus the Hamiltonian describing the system is exactly the same as in Sec. II. Therefore, finding an expression for the edge state amounts to solving the eigenvalue equation arising from the Hamiltonian in Eq. (4) with the added boundary condition $\psi(x = 0) = 0$. To the best of our knowledge, this eigenvalue problem with $\mathcal{B} \neq 0$ cannot be solved analytically for arbitrary k_y . As such, in the rest of this article we will concern ourselves with finding approximate solutions to the equation. We do this by using an approximate basis of wave functions at each value of k_y and solving the Schrödinger equation within this basis. While this basis is not exactly orthogonal, we will nevertheless find excellent agreement with the numerical results.

A. Basis for the edge-state wave function

Before we give the basis of wave functions for the edge state, it is insightful to first explain the general idea behind the construction of these wave functions. In the previous section we have found that the Landau states from Eq. (8) are solutions to the Schrödinger problem with the Hamiltonian of Eq. (4). The only problem with applying these solutions to the edge state is, of course, that they do not adhere to the hard-wall boundary condition at $x = 0$. However, we now show that we can make a modification to the Landau-state wave functions such that they adhere to the boundary conditions while still approximately solving the Schrödinger equation with remarkable accuracy. We call these modified states the Dirichlet Landau states (D-LSs), and the energy corresponding to these solutions is taken to be equal to the energy of Eq. (9) for the original LS. Looking at Fig. 1, we see that the edge state dispersion (shown in red) at multiple k_y approaches or crosses the Landau energies (dashed lines). The central idea of this paper is then as follows: when the wave number k_y is such that the energy of the edge state is close to a Landau energy, we can accurately describe the edge state wave function by the D-LS corresponding to this Landau energy. This gives us a list of specific wave numbers k_y for which we can accurately obtain the edge state. We then treat these solutions, the D-LSs, as a basis for solving the entire dispersion relation of the edge state.

For reasons that will be obvious later, it is convenient to split the D-LS basis into three distinct classes of wave functions, namely

1. Dirichlet bulk states (D-bulk),
2. Dirichlet non-normalizable Landau states (D-NLS),
3. Dirichlet complex Landau states (D-CLS).

For each class we give a brief interpretation and some physical justification in the following sections. For a full discussion and a derivation of the various classes, the reader is referred to the appendices where applicable.

The general form of the basis wave functions of each class is given by

$$\psi_{\tau_z n}^{\pm} = \mathcal{N}_{\tau_z n}^{\pm} \left(1 - e^{-\Lambda_{-}(E_{\tau_z n}^{\pm})x}\right) \begin{bmatrix} \alpha_{\tau_z n}^{\pm} \phi_{n-1}(x, k_y) \\ \beta_{\tau_z n}^{\pm} \phi_n(x, k_y) \end{bmatrix}, \quad (12)$$

where $\mathcal{N}_{\tau_z n}^{\pm}$ is a normalization constant. The energy $E_{\tau_z n}^{\pm}$ is given by Eq. (9), with different choices for n and the corresponding branch (that is, either E^+ or E^-) for each class of wave functions. We will see that for each class we either pick the $+$ or $-$ solution, and as such, we drop the superscript in those cases for clarity. The only difference between the classes lies in their choice of solution branch \pm , n , α and β , as we explain in the next sections.

It can be seen that the sole difference between the D-LSs and the “regular” Landau states is the factor $(1 - e^{-\Lambda_{-}(E_{\tau_z n, i})x})$. This is the modification we alluded to at the start of this section, and forces the hard-wall boundary condition to be satisfied. In

this factor, we have used the exponential decay parameter

$$\Lambda_-(E) = \sqrt{\frac{2D(E + k_y^2 D) - v_F^2 - F(\Delta - 2Bk_y^2) - \sqrt{R(E)}}{2(D^2 - F^2)}}, \quad (13)$$

where $R(E) = 4E^2F^2 + v_F^4 - 2F\Delta v_F^2 + D^2\Delta^2 - 4ED(v_F^2 - F\Delta)$. The derivation of this prefactor relies on the calculation of the edge state for $\mathcal{B} = 0$ T, which is explained in detail in Appendix A. In short, it can intuitively be viewed as a factor that dominates the behavior of the wave function near the edge, but changes it only marginally for $x \gg 0$.

1. Dirichlet bulk states

We refer to the first class of the basis wave functions as the Dirichlet bulk states. This name reflects that they arise directly from the bulk-state calculation in Sec. II, with a modification to adhere to the hard-wall (Dirichlet) boundary condition. As such, these wave functions have the form of Eq. (12) where the parameters α and β are given by

$$\begin{bmatrix} \alpha_{\tau_z n, \text{D-bulk}} \\ \beta_{\tau_z n, \text{D-bulk}} \end{bmatrix} = v_{\tau_z n} \quad (14)$$

as in Eq. (11). We remind that $v_{\tau_z,0} = [0, 1]^\top$ for both $\tau_z = \pm 1$. As we have seen in Sec. II, the bulk wave functions have two solution branches $v_{\tau_z n}^\pm$ for $n > 0$. This raises an obvious question, namely which branch to use for the D-bulk states. As we will discuss later in this section, we can deduce by physical arguments that for $k_y \ll 0$ the two branches of the edge state must approach the Landau energies $E_{\tau_z,0}$. By noting that the two τ_z cases must form a Dirac cone, we can deduce whether each branch goes upwards or downwards. Alternatively, and perhaps more insightfully, one can solve the edge state numerically and take note of the general shape of the dispersion relation. This is done in Fig. 1 for $\tau_z = 1$ and $\mathcal{B} = 1$ T. In this figure the edge state is shown in red, and we see that it crosses all the Landau energies of the $v_{\tau_z n}^+$ branches. As such, for $\tau_z = +1$ and $n > 0$ we use $v_{\tau_z n}^+$ and $E_{\tau_z n}^+$ in Eqs. (12) and (14). Conversely, for $\tau_z = -1$ we use $v_{\tau_z n}^-$ and $E_{\tau_z n}^-$. Since the superscript is fully determined by the sign of τ_z , we drop it for clarity.

As discussed before, we state that the wave function $\psi_{\tau_z n, \text{D-bulk}}$ from Eq. (12) is a good approximation to the true edge state for the precise k_y when its energy is equal to $E_{\tau_z n}$, that is, the k_y at which the red edge state crosses the dashed Landau level in Fig. 1. We will denote the wave number uniquely attributed to $E_{\tau_z n}$ ($n > 0$) as $k_{y,\tau_z n}$. A method of finding the set $\{k_{y,\tau_z n}\}$ via a self-consistency relation can be found in Appendix C. In brief, the wave number can be calculated from the fact that if one takes the expectation value of the Hamiltonian for these wave functions and sets it equal to a Landau energy, the wave number k_y is the only unknown in the equation. Note that this method does not rely in any way on solving the differential equation numerically. In this section we also show that Eq. (14) is a remarkably accurate approximation of the edge state wave function at $k_{y,\tau_z n}$, and thus our choice of this basis vector is justified.

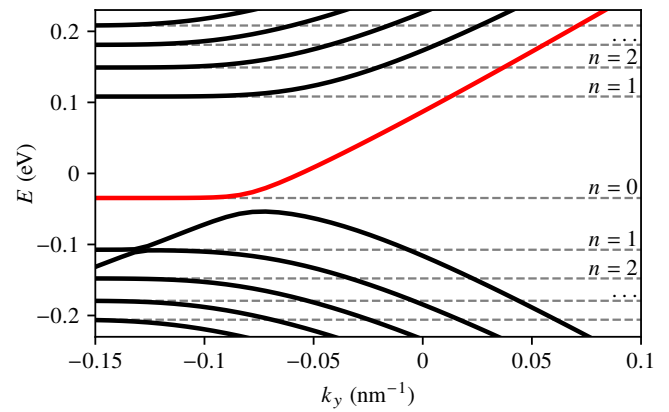


FIG. 1. Numerical calculation of the spectrum of the system for $\mathcal{B} = 1$ T and $\tau_z = +1$. For clarity, $\tau_z = -1$ is not shown. The dashed lines are the bulk LLs given by Eq. (9) for different values of n . Notice that there are two LLs for each n , except for $n = 0$. The red line corresponds to the edge state, as this is the band that forms the Dirac cone with its $\tau_z = -1$ counterpart (not shown here). It can be seen that every band acquires the bulk LL energy when $k_y \rightarrow -\infty$.

An extra comment needs to be made about the wave function $\psi_{\tau_z,0, \text{D-bulk}}$, i.e., the case $n = 0$. As can be seen in Fig. 1, the edge state never actually crosses $E_{\tau_z,0}$, but only approaches it asymptotically. To explain this behaviour, it is insightful to consider the coordinate transformation $\xi = x/l_B + k_y l_B$ that was performed to obtain the solution of the bulk Hamiltonian. We know that the Hermite function $\phi_n(x, k_y)$ as defined by Eq. (7) is localized around $\xi = 0$, and thus around $x = -k_y/l_B^2$. Therefore, for $k_y \ll 0$, the wave function is localized at $x \gg 0$. Since the Hermite functions have Gaussian decay, the wave function essentially already satisfies the Dirichlet boundary condition in this case. In other words, we expect the wave function of the edge state to be identical to the solution of the bulk Hamiltonian in the regime $k_y \ll 0$, with an identical energy. Looking at Eq. (12), it can readily be verified that for these values of k_y , we indeed have $\psi_{\tau_z,0, \text{D-bulk}}(x, k_y) = \psi_{\tau_z,0, \text{bulk}}(x, k_y)$ as the exponential term is approximately zero. The asymptotic behaviour of the edge state can then be attributed to the decaying influence of the edge at $x = 0$, which is zero in the limit $k_y \rightarrow -\infty$. Note that this implies that, as opposed to the case $n > 0$, we cannot attribute a single $k_{y,\tau_z,0}$ to the energy $E_{\tau_z,0}$. Instead, we expect the wave function $\psi_{\tau_z,0, \text{D-bulk}}$ to be a good approximation to the edge state over a large range of $k_y \ll 0$.

2. Dirichlet non-normalizable Landau states

We now draw attention to the Hermite functions in Eq. (7). The Hermite functions with $n \geq 0$ are not the only possible solutions to the diagonal components of the Hamiltonian in Eq. (6). Additionally, there are non-normalizable solutions which go to infinity for $x \rightarrow -\infty$. We call these functions the non-normalizable Hermite functions $\phi_n(x, k_y)$, with $n < 0$. In the usual treatment of the quantum harmonic oscillator these func-

tions are ignored, because they constitute non-normalizable and thus unphysical solutions. However, in the case of the edge state, these functions exist in the domain $[0, \infty)$, and are therefore normalizable. Hence, it is not unreasonable to suggest that they could manifest themselves in the functional form of the edge-state wave function for some k_y .

This observation gives rise to our second class of basis functions. There is one function for each τ_z , with $n = 0$ and $E_{\tau_z, \text{NLS}} = E_{+1,0}^+ (E_{\tau_z, \text{NLS}} = E_{-1,0}^-)$ for $\tau_z = +1 (\tau_z = -1)$, which is again calculated using Eq. (9). Note that $E_{+1, \text{NLS}} \approx -E_{+1,0}^-$ and $E_{-1, \text{NLS}} \approx -E_{-1,0}^+$, where the only reason for the approximate symbol comes from the minor effect of the Zeeman splitting. As such, the D-NLS can be viewed as the counterpart to the single $\psi_{\tau_z,0, \text{bulk}}$ with $n = 0$, similar to the two (\pm) branches of Eq. (8) for $n > 0$. The prefactors α and β are given by

$$\begin{bmatrix} \alpha_{\tau_z, \text{D-NLS}} \\ \beta_{\tau_z, \text{D-NLS}} \end{bmatrix} = \begin{bmatrix} (2e\mathcal{B}D - 2\mu\mathcal{B} + \Delta\tau_z)\sqrt{\ln 2} \\ 2v_F\sqrt{e\mathcal{B}} \end{bmatrix} \quad (15)$$

and the non-normalizable Hermite function with $n = -1$ is given by

$$\phi_{-1}(x, k_y) = \frac{2}{\sqrt{l_B\sqrt{\pi}\ln 2}} H_{-1}(\xi) e^{-\xi^2/2}, \quad (16)$$

where $H_{-1}(x) = \frac{1}{2}\sqrt{\pi}e^{x^2} \text{erfc}(x)$, with $\text{erfc}(x)$ the complementary error function. The prefactor is chosen such that the function is normalized with respect to ξ in the domain $[0, \infty)$.

Just like the functions from the first class, the wave functions in this class are good solutions when the energy of the edge state is equal to the corresponding energy of the underlying Landau state, in this case $E_{\tau_z, \text{NLS}}$. In practice this means that the wave functions of Eq. (14) are accurate solutions at discrete values for the wave number, which we will call $k_{y, \tau_z, \text{D-NLS}}$, and these values are found by the same procedure as in the previous section. An example of a D-NLS wave function is shown in the inset of Fig. 3. A full treatment of the extension of the harmonic oscillator to the regime with $n < 0$ is given in Appendix B. Furthermore, in this appendix we describe how the ladder operators from Eqs. (5) act on the non-normalizable Hermite functions and how the D-NLS arises from these functions. To the best of our knowledge, this treatment and application of the non-normalizable harmonic oscillator functions is a novel ingredient of our work.

3. Dirichlet complex Landau states

In addition to the D-NLS, it is natural to also look at Hermite functions with $n \leq -1$. The energy of the corresponding wave function is given by Eq. (9), with $n \leq -1$. This poses a problem, however, because the energy turns out to be complex for $n \leq -1$. Additionally, the eigenvectors are also complex, with $v_{\tau_z, n}^+$ the complex conjugate of $v_{\tau_z, n}^-$ for $n \leq -1$. Hence, we call these states the Dirichlet complex Landau states. We interpret this as these states not having a well-defined energy, but being spread out around the real part of this energy. Since

E_n^+ is the complex conjugate of E_n^- for all $n < 0$, i.e., the real part of the energy is degenerate, we can make a superposition of two solutions giving a state with a real energy and real wave function. For instance, the prefactors α and β for $n = -1$ are the elements of the eigenvectors $v_{\tau_z, n}^\pm$, and are given by

$$\begin{bmatrix} \alpha_{\tau_z, -1, \text{D-CLS}}^\pm \\ \beta_{\tau_z, -1, \text{D-CLS}}^\pm \end{bmatrix} = \begin{bmatrix} \Delta\tau_z + 2e\mathcal{B}(D - 2Bn\tau_z) - 2\mu\mathcal{B} \pm \sqrt{\mathcal{A}_{\tau_z, -1}} \\ 2v_F\sqrt{2e\mathcal{B}}\sqrt{\frac{\ln 4}{1 - \ln 2}} \end{bmatrix}, \quad (17)$$

where one can indeed see that $\alpha_{\tau_z, -1, \text{D-CLS}}^+$ and $\beta_{\tau_z, -1, \text{D-CLS}}^+$ are the complex conjugates of $\alpha_{\tau_z, -1, \text{D-CLS}}^-$ and $\beta_{\tau_z, -1, \text{D-CLS}}^-$ respectively. In contrast to the wave functions of other classes, which precisely follow Eq. (12), we thus have that the wave functions of the third class follow

$$\begin{aligned} \psi_{\tau_z, n, \text{D-CLS}}(x) = & \\ & \mathcal{N}_{n, \text{D-CLS}} \left((1 - e^{-\Lambda_-(E_{\tau_z, n, \text{D-CLS}}^+)x}) \begin{bmatrix} \alpha_{\tau_z, n}^+ \phi_{n-1}(x, k_y) \\ \beta_{\tau_z, n}^+ \phi_n(x, k_y) \end{bmatrix} \right. \\ & \left. + (1 - e^{-\Lambda_-(E_{\tau_z, n, \text{D-CLS}}^-)x}) \begin{bmatrix} \alpha_{\tau_z, n}^- \phi_{n-1}(x, k_y) \\ \beta_{\tau_z, n}^- \phi_n(x, k_y) \end{bmatrix} \right), \end{aligned} \quad (18)$$

which is simply a superposition of two copies of the original wave-function form, one for each sign. Notice that this wave function is real for all $n < 0$.

Since the states are presumably spread out over a range of energies, we do not assign a single value $k_{y, n, \text{D-CLS}}$ to these states, as opposed to the D-LS and D-NLS. However, in Sec. III B we will discuss how the D-CLS nonetheless influences the total approximation for the edge-state wave function. In Appendix B we discuss the functions $\phi_n(x, k_y)$ for $n \leq -1$ in more detail. We also clarify how to calculate their corresponding coefficients $\alpha_{\tau_z, n}^\pm$ and $\beta_{\tau_z, n}^\pm$ for general n , which essentially amounts to continuing the raising and lowering operators to the domain of negative integers and subsequently diagonalizing the bulk Hamiltonian of Eq. (6).

B. Basis expansion

Using the states discussed in Sec. III A, we would now like to express the total wave function of the edge state in this basis. This is straightforwardly done by making a linear superposition of the basis vectors for each possible value of k_y . However, one needs to be careful with how to implement the explicit k_y -dependence of each of the basis states in the total solution. Specifically, we have seen that the D-bulk states ($n > 0$) and D-NLS fully characterize the edge state at discrete wave numbers $k_{y, \tau_z, n}$ and $k_{y, \tau_z, \text{D-NLS}}$, respectively. Conversely, the D-bulk state ($n = 0$) and D-CLSs do not have these discrete wave numbers, as they are valid approximations (or part of a valid approximation) over a range of $k_y < k_{y, \tau_z, \text{D-NLS}}$. To address this, we make a case separation for the definition of the total wave function of the edge state as

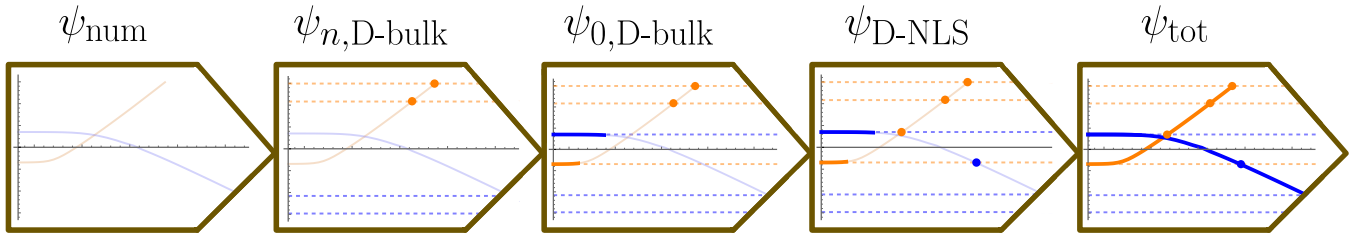


FIG. 2. Graphical summary of this work, a piecewise construction of an analytical function for the edge state. Each panel shows a dispersion relation of the one-dimensional Bi_2Se_3 edge state with the wave number k_y on the x axis. The orange (blue) colour represents the $\tau_z = +1$ ($\tau_z = -1$) edge state. In the first panel we show the numerical dispersion relation in faded colors, with wave function ψ_{num} . Full colours represent the fact that we know the analytical wave function corresponding to this k_y . Note that we use the numerical solution only for reference, as it is not used in the analytical calculation. In the second and third panel we add $\psi_{n,\text{D-bulk}}$ with $n > 0$ and $n = 0$ respectively. The dashed lines correspond to the Landau energy. In the fourth panel we add the $\psi_{\text{D-NLS}}$ at their corresponding k_y . The D-CLS is not shown here. Finally, in the last panel we interpolate between these known basis vectors as per Sec. III B to obtain the full dispersion relation, achieving the goal of this article.

$$\psi_{\tau_z,\text{tot}}(x, k_y) = \begin{cases} \sum_{i \in I_1} c_i(k_y) \psi_{\tau_z,i}(x, k_y) & \text{if } k_y < k_{y,\tau_z,\text{D-NLS}}, \\ \sum_{i \in I_2} c_i(k_y) \psi_{\tau_z,i}(x, k_y) & \text{if } k_y \geq k_{y,\tau_z,\text{D-NLS}}, \end{cases} \quad (19)$$

where I_1 is a set of indices which reflect the basis states in classes 1 ($n = 0$) and 3, and I_2 a set of indices which reflect the basis states in classes 1 ($n > 0$) and 2. Furthermore, $\psi_{\tau_z,i}$ is an element of the set of basis states as defined in Sec. III A, and $k_{y,i}$ the corresponding discrete value of the wave number associated with $\psi_{\tau_z,i}$, if it exists. We note that for $k_y < k_{y,\tau_z,\text{D-NLS}}$, we use a slightly different definition for $\psi_{\tau_z,\text{D-NLS}}$, namely one where we have not substituted $k_{y,\text{D-NLS}}$ into Eq. (12). As such, the D-NLS is in this case still dependent on k_y . One could use Eq. (19) without making this change, but we have found that this yields worse results for the total wave function. Therefore, to emphasize, in the first case, the linear superposition consists of the D-bulk state with $n = 0$, the D-CLS and D-NLS, and there is an explicit k_y -dependence in each basis vector. In the second case, the linear superposition consists of the D-bulk states with $n > 0$ and the D-NLS, and there is no k_y -dependence in each basis vector. Hence, in this case all the k_y -dependence is encapsulated into the prefactors c_i .

To calculate the coefficients c_i in Eq. (19) for a given k_y we impose that $\psi_{\tau_z,\text{tot}}(x, k_y)$ is an eigenvector of h_{τ_z} with eigenvalue $E(k_y)$, and that the expectation value of h_{τ_z} with respect of $\psi_{\tau_z,\text{tot}}(x, k_y)$ is equal to that same $E(k_y)$. This yields a linear system of equations, which together with the normalization condition determine E and all c_i . These equations are the time-independent Schrödinger equations expressed in a non-orthogonal basis, and are given by

$$\sum_j \langle \psi_i | h_{\tau_z} | \psi_j \rangle c_j = \sum_j E \langle \psi_i | \psi_j \rangle c_j, \quad (20)$$

where index j represents the components of the total wave function as in Eq. (19). Note that the matrix elements on the

right-hand side of Eq. (20) are generally nontrivial because our basis states ψ_i are in general not fully orthogonal. Once these c 's have been obtained for a single k_y , one has an analytical approximation of the edge state at that wave number without relying on the numerical solution, thereby achieving our goal.

C. Recap of method

In this section we take a step back and summarize the step-by-step recipe to arrive at the full edge-state dispersion relation, which is the core result of this paper. Given τ_z and a value of $\mathcal{B} > 0$, the steps are as follows:

1. Calculate the bulk eigenstates of Eq. (8), and construct the LL wave functions $\psi_{\tau_z n, \text{bulk}}^\pm(x, k_y)$.
2. Calculate the LL energies $E_{\tau_z n}$ up to some n using Eq. (9). Use these energies to construct $\psi_{\tau_z n, \text{D-bulk}}$ with Eq. (14) for these same n . As discussed in Appendix C, calculate the discrete values of k_y that correspond to these functions via a self-consistency relation. This yields a list of solutions to the edge-state Hamiltonian at the points $(k_{y,\tau_z n}, E_{\tau_z n})$.
3. Calculate the D-NLS according to Sec. III A 2, and find its appropriate $k_{y,\tau_z,\text{D-NLS}}$. Also calculate the D-CLS as described in Sec. III A 3.
4. Pick a k_y at which the edge-state wave function is to be computed. Propose a linear combination of the basis set of wave functions as in Eq. (19), and calculate the coefficients using Eq. (20).
5. Finally, repeat step 4 for many k_y to obtain the full dispersion relation.

A graphical summary of the recap, represented as the piecewise construction of the dispersion relation is shown in Fig. 2. Regarding step 4, we remind that one has the freedom to choose how many wave functions are taken into account for the linear combination in Eq. (19). We recommend the following:

- For $k_y < k_{y,\tau_z,\text{D-NLS}}$, include three functions: $\psi_{\tau_z,0,\text{D-bulk}}$, $\psi_{\tau_z,\text{D-NLS}}$ and $\psi_{\tau_z,\text{D-CLS}}$.
- For $k_{y,\tau_z,\text{D-NLS}} \leq k_y < k_{y,\tau_z,1}$, include two functions: $\psi_{\tau_z,\text{D-NLS}}$ and $\psi_{\tau_z,1,\text{D-LS}}$.

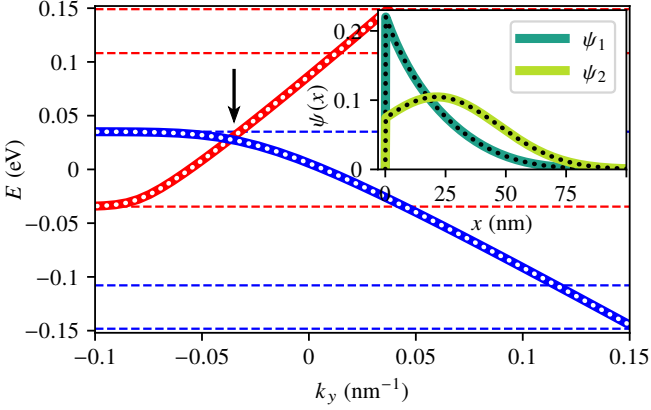


FIG. 3. Dispersion relation of the edge state at $\mathcal{B} = 1$ T. The white dots are the numerical solutions while the full lines are obtained via the method described in Sec. III C. The red and blue lines correspond to $\tau_z = +1$ and $\tau_z = -1$, respectively. The dashed lines indicate the energies of the different LLs. It can be seen that our method agrees extremely well with the numerical solution. The inset shows the wave function of the D-NLS with $\tau_z = 1$ at the point indicated by the black arrow, with ψ_1 and ψ_2 the first and second component of the wave function, respectively. The black dots show the numerical calculation and the solid lines correspond to our approximation.

- For $k_y \geq k_{y,1}$, include two functions: $\psi_{\tau_z n, \text{D-LS}}$ and $\psi_{\tau_z, n+1, \text{D-LS}}$ such that $k_{y, \tau_z n} \leq k_y < k_{y, \tau_z, n+1}$.

We have found that this convention yields excellent results, and we will use it in the rest of the article.

IV. RESULTS OF THE MODEL

In this section we first compare the method as described in the last section to the numerical solution of the differential equation. The case we discuss is the edge state with $\mathcal{B} = 1$ T. At the end of this section we use the analytical method to obtain experimentally observable STM spectra.

In Fig. 3 we show the dispersion relation obtained via this method. The dotted lines correspond to numerical simulations, while the full lines correspond to the wave function obtained via our analytical method. The dispersion relations match almost perfectly, and in fact the error never exceeds 0.15 meV. Fig. 4 shows the total difference between wave functions of the two methods for all values of k_y . This error is calculated as $\int_0^\infty dx \|\psi_{\text{num}}(x) - \psi(x)\|^2$ and is seen to be very small everywhere. The inset of Fig. 4 shows the worst performing wave function for $\mathcal{B} = 1$ T, which is at $k_y = -0.012 \text{ nm}^{-1}$ and $\tau_z = +1$. Even at this point, the approximation is very close to the numerical solution. Therefore, we conclude that our method yields a good approximation of the exact solution for both the energy and wave function at this magnetic field. We have found similar results for all $\mathcal{B} \in [0.1, 10]$ T.

Fig. 3 also shows that the two τ_z branches behave asymmetrically. This is due to the broken particle-hole symmetry in the system, which manifests in the Hamiltonian of Eq. (4) due to the addition of a diagonal momentum-dependent term.

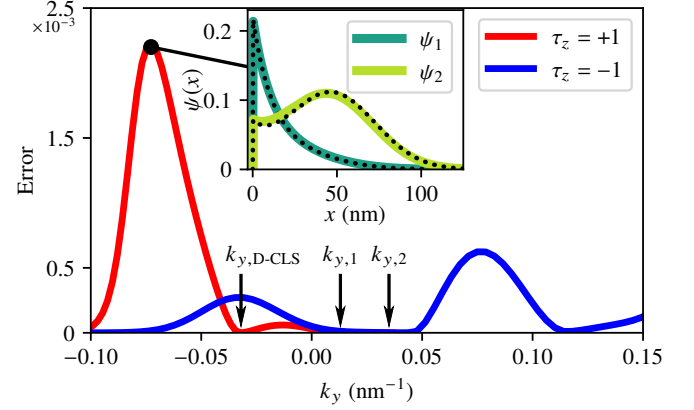


FIG. 4. L^2 difference between the numerical solution and our analytical approximation, i.e., $\int_0^\infty dx \|\psi_{\text{num}}(x) - \psi(x)\|^2$. The red and blue lines correspond to $\tau_z = +1$ and $\tau_z = -1$, respectively. We draw attention to the fact that the error is almost exactly zero when $k_y = k_{y, \text{D-NLS}}$, $k_{y,1}$, $k_{y,2}$, etc., namely when the energy is equal to that of a LL, shown by the arrows for τ_z . (cf. Fig. 3). The inset shows the comparison at the attached highest-error point and reveals that even in this case the approximation is very accurate.

The nonzero D effectively pushes the Dirac point upwards in energy, causing the dispersion relation of the edge state to become asymmetric around $E = 0$.

Fig. 5 shows the evolution of the coefficients c_i introduced in Eq. (19) as a function of k_y for $\mathcal{B} = 1$ T and $\tau_z = +1$. Each colour represents the c_i corresponding to a different wave function $\psi_{\tau_z, i}$. We see that the coefficients are continuous in k_y , meaning that the edge-state wave function continuously interpolates from one basis vector to the next. We also see that the D-CLS plays a sizable role in the full wave function for a certain range of k_y . If we do not include this wave function, we have found noticeably worse results, especially near the Γ point of the dispersion relation. Therefore, even though there is no single k_y at which the D-CLS fully determines the edge state, it cannot be ignored in the total wave function.

In a similar fashion, we see that there is a range of wave numbers around $k_y = -0.035 \text{ nm}^{-1}$ at which $\psi_{\text{D-NLS}}$ is dominant, and even a single value at which it fully determines the wave function, practically without any error (see also Fig. 4). This is conclusive evidence that this wave function, and thus the negative order Hermite functions, cannot be ignored in the treatment of this system.

Finally, we show in Fig. 6 the local density of states (LDOS) of the edge state in a 1 T magnetic field, as observable in STM measurements. Readily identifiable are the two bulk energies, around ± 0.035 eV, which correspond to the edge state at very negative wave numbers. By comparing the LDOS of this article with experimentally obtained data, one could verify the validity of our analytic approximation.

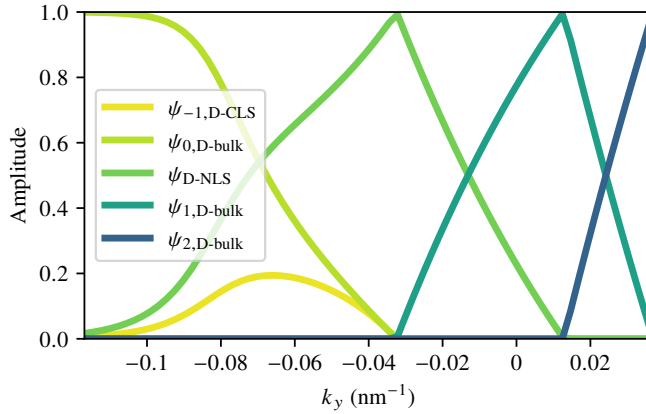


FIG. 5. Parameters c_i from Eq. (19) for the wave functions with $B = 1$ T and $\tau_z = 1$. Each colour represents a different part of the wave function. Notice that since this basis is in general not exactly orthonormal, the squared factors at a single k_y do not necessarily add up to one. It can be seen that at $k_y = k_{y,D-NLS}, k_{y,0}, k_{y,1}$ the full wave function consists solely of a single component. Notice the sizable contribution of $\psi_{-1,D-CLS}$.

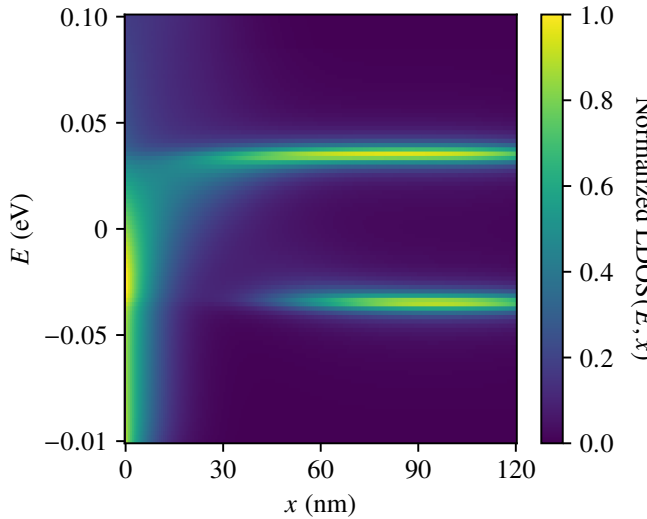


FIG. 6. Calculation of the local density of states (LDOS) for the edge state in Bi_2Se_3 via our method in a perpendicular magnetic field of 1 T. The LDOS measurement is modeled as a Cauchy (Lorentzian) distribution with $\gamma = 7.5$ meV. Two Landau levels can be clearly identified at $E = \pm 35$ meV eV.

V. CONCLUSION AND OUTLOOK

In this article we have derived an analytical description of the edge-state wave functions of a Bi_2Se_3 nanosheet under a

perpendicular magnetic field as a function of the wave number k_y . The approximation is based on the observation that the edge state wave function inherits the form of the Landau states when the energy is equal to the corresponding Landau energy. Furthermore, we have introduced the D-NLS and D-CLS, which are usually non-normalizable bulk-like states appearing solely due to the presence of the edge, and are constructed from negative order Hermite functions. We have shown that they are crucial to describe the edge state in the energy range corresponding to the bulk band gap. Using these states, we have devised an analytical description of the wave function for general k_y . This yields very accurate results that agree with numerical calculations.

Our analytical description enables subsequent calculations that can shed light on the nature of the edge state and its behavior under external fields and perturbations. For example, one can derive an effective Hamiltonian for the nanosheet edge state in a perpendicular magnetic field that can be used for a detailed study of the edge physics alone and as a starting point for the detailed study of impurity scattering. Furthermore, we can investigate the behavior of the Dirac point of the system for high values of the magnetic field. Our calculation shows that time-reversal symmetry is not necessary to explain the robustness of the edge state. We argue that even though time-reversal symmetry is broken, the perpendicular magnetic field does not couple the two helical modes to each other. As such, scattering between them is impossible and the edge state remains robust. One possible area of further research is to consider a magnetic field with an in-plane component. This magnetic field would couple the two modes together, presumably killing the edge state, similar to the effect of magnetic impurities [25]. We hope that our work stimulates more experimental work on these exciting features of topological edge states.

ACKNOWLEDGMENTS

We thank Daniel Vanmaekelbergh and Ingmar Swart for useful discussions about the experiments. This work is supported by the research program “Materials for the Quantum Age” (QuMat). This program (registration number 024.005.006) is part of the Gravitation program financed by the Dutch Ministry of Education, Culture and Science (OCW).

- [1] I. Žutić, J. Fabian, and S. D. Sarma, Spintronics: Fundamentals and applications, *Reviews of Modern Physics* **76**, 323 (2004).
- [2] M. Z. Hasan and J. E. Moore, Three-dimensional topological insulators, *Annu. Rev. Condens. Matter Phys.* **2**, 55 (2011).
- [3] B. A. Bernevig, *Topological insulators and topological superconductors* (Princeton University Press, 2013).
- [4] D. Pesin and A. MacDonald, Quantum kinetic theory of current-induced torques in Rashba ferromagnets, *Physical Review B* **86**,

014416 (2012).

[5] J. E. Moore, The birth of topological insulators, *Nature* **464**, 194 (2010).

[6] M. E. Cage, K. Klitzing, A. Chang, F. Duncan, M. Haldane, R. B. Laughlin, A. Pruisken, and D. Thouless, *The quantum Hall effect* (Springer Science & Business Media, 2012).

[7] Y. Xia, D. Qian, D. Hsieh, L. Wray, A. Pal, H. Lin, A. Bansil, D. Grauer, Y. S. Hor, R. J. Cava, *et al.*, Observation of a large-gap topological-insulator class with a single Dirac cone on the surface, *Nature physics* **5**, 398 (2009).

[8] D. Hsieh, Y. Xia, D. Qian, L. Wray, J. Dil, F. Meier, J. Osterwalder, L. Patthey, J. Checkelsky, N. P. Ong, *et al.*, A tunable topological insulator in the spin helical Dirac transport regime, *Nature* **460**, 1101 (2009).

[9] K. Mazumder and P. M. Shirage, A brief review of Bi_2Se_3 based topological insulator: From fundamentals to applications, *Journal of Alloys and Compounds* **888**, 161492 (2021).

[10] I. Aguilera, C. Friedrich, and S. Blügel, Many-body corrected tight-binding Hamiltonians for an accurate quasiparticle description of topological insulators of the Bi_2Se_3 family, *Physical Review B* **100**, 155147 (2019).

[11] X.-L. Qi and S.-C. Zhang, The quantum spin Hall effect and topological insulators, *Physics Today* **63**, 33 (2010).

[12] O. V. Yazyev, J. E. Moore, and S. G. Louie, Spin Polarization and Transport of Surface States in the Topological Insulators Bi_2Se_3 and Bi_2Te_3 from First Principles, *Physical Review Letters* **105**, 266806 (2010).

[13] O. Chiatti, C. Riha, D. Lawrenz, M. Busch, S. Dusari, J. Sánchez-Barriga, A. Mogilatenko, L. V. Yashina, S. Valencia, A. A. Ünal, *et al.*, 2D layered transport properties from topological insulator Bi_2Se_3 single crystals and micro flakes, *Scientific Reports* **6**, 1 (2016).

[14] J. Linder, T. Yokoyama, and A. Sudbø, Anomalous finite size effects on surface states in the topological insulator Bi_2Se_3 , *Physical Review B* **80**, 205401 (2009).

[15] L. Maisel Licerán, S. J. H. Koerhuis, D. Vanmaekelbergh, and H. T. C. Stoof, Topology of Bi_2Se_3 nanosheets, *Physical Review B* **109**, 195407 (2024).

[16] M. Z. Hasan and C. L. Kane, Colloquium: topological insulators, *Reviews of Modern Physics* **82**, 3045 (2010).

[17] C.-X. Liu, H. Zhang, B. Yan, X.-L. Qi, T. Frauenheim, X. Dai, Z. Fang, and S.-C. Zhang, Oscillatory crossover from two-dimensional to three-dimensional topological insulators, *Physical Review B* **81**, 041307 (2010).

[18] H.-Z. Lu, W.-Y. Shan, W. Yao, Q. Niu, and S.-Q. Shen, Massive dirac fermions and spin physics in an ultrathin film of topological insulator, *Physical Review B—Condensed Matter and Materials Physics* **81**, 115407 (2010).

[19] Y. Zhang, K. He, C.-Z. Chang, C.-L. Song, L.-L. Wang, X. Chen, J.-F. Jia, Z. Fang, X. Dai, W.-Y. Shan, *et al.*, Crossover of the three-dimensional topological insulator Bi_2Se_3 to the two-dimensional limit, *Nature Physics* **6**, 584 (2010).

[20] M. Neupane, A. Richardella, J. Sánchez-Barriga, S. Xu, N. Alidoust, I. Belopolski, C. Liu, G. Bian, D. Zhang, D. Marchenko, *et al.*, Observation of quantum-tunnelling-modulated spin texture in ultrathin topological insulator Bi_2Se_3 films, *Nature communications* **5**, 3841 (2014).

[21] J. R. Moes, J. F. Vliem, P. M. de Melo, T. C. Wigmans, A. R. Botello-Méndez, R. G. Mendes, E. F. van Brenk, I. Swart, L. Maisel Licerán, H. T. Stoof, *et al.*, Characterization of the Edge States in Colloidal Bi_2Se_3 Platelets, *Nano Letters* **24**, 5110 (2024).

[22] C. L. Kane and E. J. Mele, \mathbb{Z}_2 topological order and the quantum spin Hall effect, *Physical Review Letters* **95**, 146802 (2005).

[23] H. Zhang, C.-X. Liu, X.-L. Qi, X. Dai, Z. Fang, and S.-C. Zhang, Topological insulators in Bi_2Se_3 , Bi_2Te_3 and Sb_2Te_3 with a single Dirac cone on the surface, *Nature physics* **5**, 438 (2009).

[24] S.-B. Zhang, Y.-Y. Zhang, and S.-Q. Shen, Robustness of quantum spin Hall effect in an external magnetic field, *Physical Review B* **90**, 115305 (2014).

[25] J. R. Moes, *From atom to edge: The influence of a magnetic field on nanoscale systems*, PhD thesis, Utrecht University (2024).

[26] R. S. Mong and V. Shivamoggi, Edge states and the bulk-boundary correspondence in Dirac Hamiltonians, *Physical Review B* **83**, 125109 (2011).

[27] B. Zhou, H.-Z. Lu, R.-L. Chu, S.-Q. Shen, and Q. Niu, Finite size effects on helical edge states in a quantum spin-Hall system, *Physical Review Letters* **101**, 246807 (2008).

[28] C.-X. Liu, X.-L. Qi, H. Zhang, X. Dai, Z. Fang, and S.-C. Zhang, Model Hamiltonian for topological insulators, *Physical Review B* **82**, 045122 (2010).

[29] W.-Y. Shan, H.-Z. Lu, and S.-Q. Shen, Effective continuous model for surface states and thin films of three-dimensional topological insulators, *New Journal of Physics* **12**, 043048 (2010).

[30] M. Rushka and J. Freericks, A completely algebraic solution of the simple harmonic oscillator, *American Journal of Physics* **88**, 976 (2020).

[31] DLMF, *NIST Digital Library of Mathematical Functions*, '<https://dlmf.nist.gov/18.17.E4>', Release 1.2.2 of 2024-09-15".

Appendix A: Edge-state solution for $B_z = 0$

In this section we find the wave function of the edge state without a magnetic field. For the Hamiltonian of Eq. (3) one can plug in the ansatz $\psi(x) = \mathbf{v}e^{-\Lambda x}$, with \mathbf{v} a two-component vector. This yields four solutions with nontrivial \mathbf{v} , of which two are normalizable. The full solution is a superposition given by

$$\psi_{B_z=0}(x) = A\mathbf{v}_{\Lambda_-}e^{-\Lambda_-(E)x} + B\mathbf{v}_{\Lambda_+}e^{-\Lambda_+(E)x}. \quad (\text{A1})$$

The Λ 's are given by

$$\Lambda_{\pm}(E) = \sqrt{\frac{2D(E + k_y^2 D) - v_F^2 \pm F(\Delta - 2Bk_y^2) \pm \sqrt{R(E)}}{2(D^2 - F^2)}}, \quad (\text{A2})$$

where $R(E) = 4E^2F^2 + v_F^42F\Delta v_F^2 + D^2\Delta^2 - 4ED(v_F^2 - F\Delta)$. The eigenvectors are given by

$$\mathbf{v}_{\Lambda_{\pm}} = \begin{pmatrix} \tau_z(\Delta/2 + B\Lambda_{\pm}^2) + E - D\Lambda_{\pm}^2 \\ v_F\Lambda_{\pm} \end{pmatrix}. \quad (\text{A3})$$

The energy E and prefactors A and B can be numerically obtained from the boundary condition $\psi(0) = 0$ and normalization. Hence, in the $B_z = 0$ case the solution is a sum of two decaying exponentials. It can be verified that for the parameter values of Bi_2Se_3 (Sec. II) we find $\Lambda_- > \Lambda_+$. As such, the behaviour around $x = 0$ is governed by Λ_- , i.e. $\psi_{B_z=0}(x \approx 0) = \tilde{\mathbf{v}}(e^{-\Lambda_- x} - 1)$, where $\tilde{\mathbf{v}} = A\mathbf{v}_+ = B\mathbf{v}_-$. This has an important implication for the wave function of the edge state with nonzero magnetic field. One may notice that the

magnetic field almost does not change the Hamiltonian if we were looking very close to the edge, i.e., for $x \approx 0$. The only difference is the term $\mu_e B_z \sigma_z$, which just shifts the diagonal terms. Therefore, we argue that close to the edge, we can ignore the effect of the magnetic field, and we retrieve a wave function that resembles the $\mathcal{B} = 0$ case. Therefore, if we have a solution of the Hamiltonian with magnetic field that does not adhere to the boundary condition at $x = 0$, we can multiply this solution with the factor $(1 - e^{-\Lambda_{-(E)}x})$ to presumably get a very close approximation of the true edge state at energy E . This insight is how we constructed Eq. (12), and we will see in the following sections that it indeed provides remarkably good solutions to the Hamiltonian.

Appendix B: Negative order Hermite functions

We have seen in the main text that to accurately describe the edge state, we need the Hermite functions with order $n < 0$. In this section, we give a derivation for these functions, and we see under which conditions they solve the Hamiltonian in Eq. (4).

1. Negative order Hermite polynomials

To derive the Hermite polynomials with negative index, our first instinct may be to look at the recurrence relation for the polynomials, which is given by

$$H_{n+1}(x) = 2xH_n(x) - 2nH_{n-1}(x). \quad (B1)$$

However, it is obvious that we are unable to calculate $H_{-1}(x)$ from $H_0(x)$ and $H_1(x)$, since this function gets cancelled for $n = 0$. Luckily, there is another recurrence relation in integral form given by

$$\int_0^x e^{-y^2} H_n(y) dy = H_{n-1}(0) - e^{-x^2} H_{n-1}(x), \quad (B2)$$

which is not as troublesome [31]. Plugging in $n = 0$ yields

$$\int_0^x e^{-y^2} dy = H_{-1}(0) - e^{-x^2} H_{-1}(x),$$

where we recognise the integral as $\frac{\sqrt{\pi}}{2} \text{erf}(x)$, with $\text{erf}(x)$ the error function. We now make the substitution $H_{-1}(x) = e^{x^2} f(x)$, which after some rearrangements yields

$$f(x) - f(0) = -\frac{\sqrt{\pi}}{2} \text{erf}(x).$$

This is solved by

$$f(x) = \frac{\sqrt{\pi}}{2} (1 - \text{erf}(x)) = \frac{\sqrt{\pi}}{2} \text{erfc}(x),$$

where $\text{erfc}(x) = 1 - \text{erf}(x)$ is the complementary error function. This gives us as a final result for the Hermite polynomial

$$H_{-1}(x) = \frac{\sqrt{\pi}}{2} e^{x^2} \text{erfc}(x). \quad (B3)$$

As a sanity check, we can verify that this function solves the characteristic differential equation for Hermite polynomials

$$\frac{d^2 H_n(x)}{dx^2} - 2x \frac{dH_n(x)}{dx} + 2nH_n(x) = 0 \quad (B4)$$

for $n = -1$.

With $H_{-1}(x)$ determined, we can easily obtain all other Hermite polynomials with negative index with the help of Eq. (B1). The first few are given by

$$H_{-1}(x) = \frac{1}{2} \sqrt{\pi} e^{x^2} \text{erfc}(x), \quad (B5a)$$

$$H_{-2}(x) = \frac{1}{2} \left(1 - \sqrt{\pi} e^{x^2} x \text{erfc}(x) \right), \quad (B5b)$$

$$H_{-3}(x) = \frac{1}{8} \left(\sqrt{\pi} (2x^2 + 1) e^{x^2} \text{erfc}(x) - 2x \right). \quad (B5c)$$

While these functions are not polynomials, to avoid confusion we group them with the positive index functions and call them all Hermite polynomials.

2. Non-normalizable bulk solutions

We know the Hermite functions for $n \geq 0$ have the shape $\phi_n(x) \propto H_n(x) e^{-x^2/2}$, so it is reasonable to suggest that this could also be true for $n < 0$. With the Hermite polynomials from last section in hand, we see that on the domain $(-\infty, \infty)$ these functions are non-normalizable for all $n < 0$, which is why they are not included in the usual treatment of the regular harmonic oscillator. However, we are studying the domain $[0, \infty)$, and in this case, these functions are normalizable. Therefore, we cannot rule out that they play a role in the semi-infinite system.

We will now prove that $H_n(x) e^{-x^2/2}$ with $n < 0$ indeed solves the diagonal part of the Hamiltonian of Eq. (4). For ease of notation we will assume $k_y = 0$ and $l_B = 1$. The final results are easily converted to solutions with general k_y and l_B . Since we are looking at the extensions of the bulk solutions, we do not impose any boundary conditions except normalizability over x from 0 to ∞ . From Sec. II A, we know that if we have a solution $\phi_n(x)$ to $(\hat{a}^\dagger \hat{a} + \frac{1}{2})$, then $\hat{a}\phi_n(x) \propto \phi_{n-1}$ is another solution. We remind that \hat{a}^\dagger and \hat{a} are the creation and annihilation operators, respectively. However, since by definition $\hat{a}\phi_0 = 0$, we cannot directly obtain $\phi_{-1}(x)$ from the positive n solutions. Therefore, we will be inspired by Eq. (7) to assume $\phi_{-1}(x) = N_{-1} H_{-1}(x) e^{-x^2/2}$, and show that it is an eigenfunction of the differential equation

$$\frac{1}{2} \left(x^2 - \frac{d^2}{dx^2} \right) \phi_{-1}(x) = \lambda_{-1} \phi_{-1}(x). \quad (B6)$$

Keeping in mind that

$$\frac{d}{dx} \text{erfc}(x) = \frac{2}{\sqrt{\pi}} e^{-x^2},$$

it is easy to show that this is indeed the case, and that the function has an eigenvalue of $\lambda_{-1} = -\frac{1}{2}$. We can calculate the

normalisation factor N_{-1} by integrating this function over x from 0 to ∞ , after which we conclude

$$\phi_{-1}(x) = \frac{2}{\sqrt{\ln(2)\sqrt{\pi}}} H_{-1}(x) e^{-\frac{x^2}{2}}. \quad (\text{B7})$$

After getting this foothold in the realm of the negative n , we can construct all the other functions using

$$\phi_n(x) = A_n (\hat{a}_-)^{-n-1} \phi_{-1}(x) \quad \forall n < 0, \quad (\text{B8})$$

where A_n is a normalisation factor dependent on n , as of yet only known for $n = -1$. From the commutation relation of the ladder operators and Eq. (B1) we can deduce that $\phi_n(x) \propto H_n(x) e^{-x^2/2}$ is indeed a solution for negative n as well, with only the prefactor A_n to be determined. In theory, if we normalise each wave function by hand, Eq. (B8) is enough to obtain everything we need to construct the D-NLS and D-CLS. However, it is more insightful to take a closer look at how the ladder operators behave with these negative order Hermite functions on the domain $[0, \infty)$.

3. Ladder operators on the semi-infinite domain

We know that the ladder operators act on a state $\phi_n(x)$ such that $\hat{a}_\pm \phi_n(x) \propto \phi_{n\pm1}(x)$, but for negative n we do not know yet what the prefactor for this operation is. We define

$$\hat{a}^\dagger \phi_n(x) = c_n \phi_{n+1}(x), \quad (\text{B9a})$$

$$\hat{a} \phi_n(x) = d_n \phi_{n-1}(x) \quad (\text{B9b})$$

and we want to find an expression for c_n and d_n for negative n . Of course, $c_n = \sqrt{n+1}$ and $d_n = \sqrt{n}$ for $n \geq 0$. We start by considering the integral

$$\int_0^\infty (\hat{a} \phi_n(x))^* (\hat{a} \phi_n(x)) dx = |d_n|^2, \quad (\text{B10})$$

where we have used Eq. (B9b) and the knowledge that ϕ_{n-1} should be normalised on $[0, \infty)$. Furthermore, using Eq. (5), we can partially integrate Eq. (B10) to obtain

$$|d_n|^2 = \frac{1}{\sqrt{2}} [(\hat{a} \phi_n(x))^* \phi_n(x)]_0^\infty + \int_0^\infty (\hat{a}^\dagger \hat{a} \phi_n)^* \phi_n dx. \quad (\text{B11})$$

It is important to draw our attention for a moment to the boundary term in Eq. (B11). Notice that it cancels for positive n for both the $(-\infty, \infty)$ and $[0, \infty)$ domain. This is because $\phi_n(x)$ must be normalisable for all n , so it must vanish at $\pm\infty$. Furthermore, for $n > 0$ either $\phi_n(x)$ or $\phi_{n-1}(x)$ is an odd function, and hence the product must be zero at $x = 0$. However, as we will later see, this is *not* the case for $n < 0$, and thus the boundary term cannot be ignored.

To continue the calculation, we identify

$$\hat{a}^\dagger \hat{a} \phi_n = n \phi_n, \quad (\text{B12})$$

which we can deduce from expression (B8) and the commutation relation $[\hat{a}, \hat{a}^\dagger] = 1$, to arrive at the final expression

$$|d_n|^2 = n - \frac{1}{\sqrt{2}} [(\hat{a} \phi_n(x))^* \phi_n(x)] \Big|_{x=0}.$$

Doing a similar calculation for c_n yields

$$|c_n|^2 = n + 1 + \frac{1}{\sqrt{2}} [(\hat{a}^\dagger \phi_n(x))^* \phi_n(x)] \Big|_{x=0}.$$

Notice that this result is consistent with the ladder operators for $n \geq 0$. We still have the freedom of choosing a phase factor for c_n and d_n . The only restriction for this choice is that it must be consistent with Eq. (B12), and thus we enforce $c_{n-1} d_n = n$. A suitable choice for $n = -1$ is

$$c_{-1} = \sqrt{2} \sqrt{\frac{1}{\sqrt{2}} [(\hat{a}^\dagger \phi_{-1}(x))^* \phi_{-1}(x)]} \Big|_{x=0}, \quad (\text{B13a})$$

$$d_{-1} = -\sqrt{-1 - \frac{1}{\sqrt{2}} [(\hat{a} \phi_{-1}(x))^* \phi_{-1}(x)]} \Big|_{x=0}, \quad (\text{B13b})$$

and for $n \neq -1$

$$c_n = \sqrt{n+1 + \frac{1}{\sqrt{2}} [(\hat{a}^\dagger \phi_n(x))^* \phi_n(x)]} \Big|_{x=0}, \quad (\text{B14a})$$

$$d_n = \text{sgn}(n) \sqrt{n - \frac{1}{\sqrt{2}} [(\hat{a} \phi_n(x))^* \phi_n(x)]} \Big|_{x=0}, \quad (\text{B14b})$$

where we have used the sign function instead of a minus sign to make the expression consistent with $n \geq 0$. These prefactors ensure normalization for the wave functions, and can be used to calculate all wave functions according to Eq. (B8). The first few Hermite functions are given by (after reintroducing k_y and l_B)

$$\phi_{-1}(x) = \frac{2}{\sqrt{\ln(2)l_B\sqrt{\pi}}} H_{-1}(\xi) e^{-\xi^2/2}, \quad (\text{B15a})$$

$$\phi_{-2}(x) = \frac{2\sqrt{2}}{\sqrt{(1-\ln 2)l_B\sqrt{\pi}}} H_{-2}(\xi) e^{-\xi^2/2}, \quad (\text{B15b})$$

$$\phi_{-3}(x) = \frac{8}{\sqrt{(2\ln 2 - 1)l_B\sqrt{\pi}}} H_{-3}(\xi) e^{-\xi^2/2}, \quad (\text{B15c})$$

where we remind that $\xi = x/l_B + k_y l_B$, and all the wave functions are normalized from $\xi = 0$ to $\xi = \infty$.

A comment needs to be made about the case separation for $n = -1$. The separation stems from the fact that in Sec. II A we defined $\phi_0(x)$ as normalized over $(-\infty, \infty)$, while $\phi_{-1}(x)$ is normalized over $(0, \infty)$. To address this mismatch in definition, c_{-1} needs to have an extra factor $\sqrt{2}$, to make sure that Eqs. (B14), (B15), and (7) are all consistent with this difference in normalization range. Alternatively, we could have avoided this mismatch by imposing that the Hermite functions from Eq. (7) must be normalized from $\xi = 0$ to $\xi = \infty$. This would have effectively only changed the numerical value of

$N_{\tau_z n}^\pm$ in Eq. (12). However, for the sake of consistency with the regular harmonic oscillator, we choose not to do this, and instead solve the issue by simply changing c_{-1} . Note that this only plays a role in the calculation of $[\alpha_{\tau_z, \text{D-NLS}}, \beta_{\tau_z, \text{D-NLS}}]^\top$ in Sec. III A 2, as this calculation uses an Ansatz with both ϕ_0 and ϕ_{-1} and thus c_{-1} enters the equation.

The first few values of c_n and d_n are shown in Table I. For $n < 0$ these prefactors seem to follow the pattern

$$c_n = \sqrt{1 + \delta_{n,-1}} \sqrt{n + 1 + \frac{(-1)^n}{C_n - \ln(2)}}, \quad (\text{B16a})$$

$$d_n = -\sqrt{n + \frac{(-1)^n}{C_n - \ln(2)}}, \quad (\text{B16b})$$

with

$$C_n = \sum_{i=1}^{-n-1} \frac{(-1)^{i+1}}{i}, \quad (\text{B17})$$

where we note that $C_0 = 0$. We have found that Eqs. (B16) are correct to *at least* $n = -50$, but we have not proven the general case.

With the explicit values of c_n and d_n in hand, we can now diagonalize the bulk Hamiltonian from Eq. (6) with the Ansatz from Eq. (8), where now $n < 1$ is allowed. In particular, for $n = 0$ this yields $[\alpha_{\tau_z, 0}^\pm, \beta_{\tau_z, 0}^\pm]^\top = [0, 1]^\top$ and Eq. (15), while for $n = -1$ this yields Eq. (17).

TABLE I. Prefactors of the ladder operators for negative index.

n	c_n	d_n
-1	$\sqrt{\frac{2}{\ln 2}}$	$-\sqrt{\frac{1}{\ln 2} - 1}$
-2	$\sqrt{\ln 2 - 1}$	$-\sqrt{\frac{1}{1 - \ln 2} - 2}$
-3	$\sqrt{\frac{2}{\ln 4 - 1} - 2}$	$-\sqrt{\frac{2}{\ln 4 - 1} - 3}$
-4	$\sqrt{\frac{6}{5 - 3 \ln 4} - 3}$	$-\sqrt{\frac{6}{5 - 3 \ln 4} - 4}$
-5	$\sqrt{\frac{12}{6 \ln 4 - 7} - 4}$	$-\sqrt{\frac{12}{6 \ln 4 - 7} - 5}$

Appendix C: Wave functions at discrete k_y

In Sec. III A we claimed that the wave functions $\psi_{\tau_z, \text{D-NLS}}$ and $\psi_{\tau_z n, \text{D-bulk}}$ ($n > 0$) are good approximations at discrete values of the energy. In this section we explain how to obtain the k_y 's corresponding to these energies, and show that it indeed leads to good approximate wave functions.

We start by noting that since the wave functions under consideration are derived from (possibly non-normalizable) bulk states, we can attribute to each wave function the Landau energy in Eq. (9) that corresponds to the appropriate bulk state. We denote these wave functions as $\psi_{\tau_z n, i}$ and their corresponding energy as $E_{\tau_z n, i}$, where i is an index that denotes the wave function class (D-bulk or D-NLS). Note that we can absorb the superscript \pm of the Landau energy into the index n for both the D-bulk and the D-NLS, as is discussed in Sec. III A. Since, presumably, the wave functions are good solutions at this energy, the expectation value of Hamiltonian (4) must be equal to the same energy, and thus

$$\langle \psi_{\tau_z n, i}(x, k_y) | h_{\tau_z}(k_y) | \psi_{\tau_z n, i}(x, k_y) \rangle = E_{\tau_z n, i}. \quad (\text{C1})$$

In this equation, the only unknown is k_y , which we can numerically solve for. This yields the specific $k_{y, \tau_z, i}$ at which wave function $\psi_{\tau_z n, i}(x, k_y)$ is a good solution to the Schrödinger equation. Note that this method does not rely in any sense on discretizing and numerically solving the Schrödinger equation for the edge state. As such, instead of numerical solutions, the wave functions should be thought of as analytic approximations or variational solutions.

A comparison of the wave functions $\psi_{+1, n, \text{D-bulk}}$ for various magnetic fields and n is shown in Fig. 7. It can be seen that the wave function is practically indistinguishable from the numerical solution. We have found similar results for $\tau_z = -1$, and the wave functions $\psi_{\tau_z, \text{D-NLS}}$.

It should be noted that for the wave function at certain energies, Eq. (C1) yields multiple solutions for k_y . This can be understood by considering Fig. 1. If we look for example at the positive Landau level with $n = 2$, we see that, apart from the edge state, the energy is crossed by a higher energy band as well. We have found that in this case the wave function $\psi_{\tau_z, 2, \text{D-LS}}(x, k_y)$ does not only describe the edge state correctly, but also, if we take the extra solution for k_y , this higher lying state. This was true for all n that we checked (up to $n = 10$) for both τ_z . An analytic function for all the energy bands should be obtainable via a procedure similar to that we applied for the edge state, but this lies outside the scope of this article. For our purpose, we just need the insight that if multiple states cross a certain Landau energy, the crossing with the highest wave number corresponds to the edge state, as can be seen in Fig. 1. Therefore, if Eq. (C1) returns more than one solution for k_y , it is this highest wave number that we identify as $k_{y, \tau_z n, i}$.

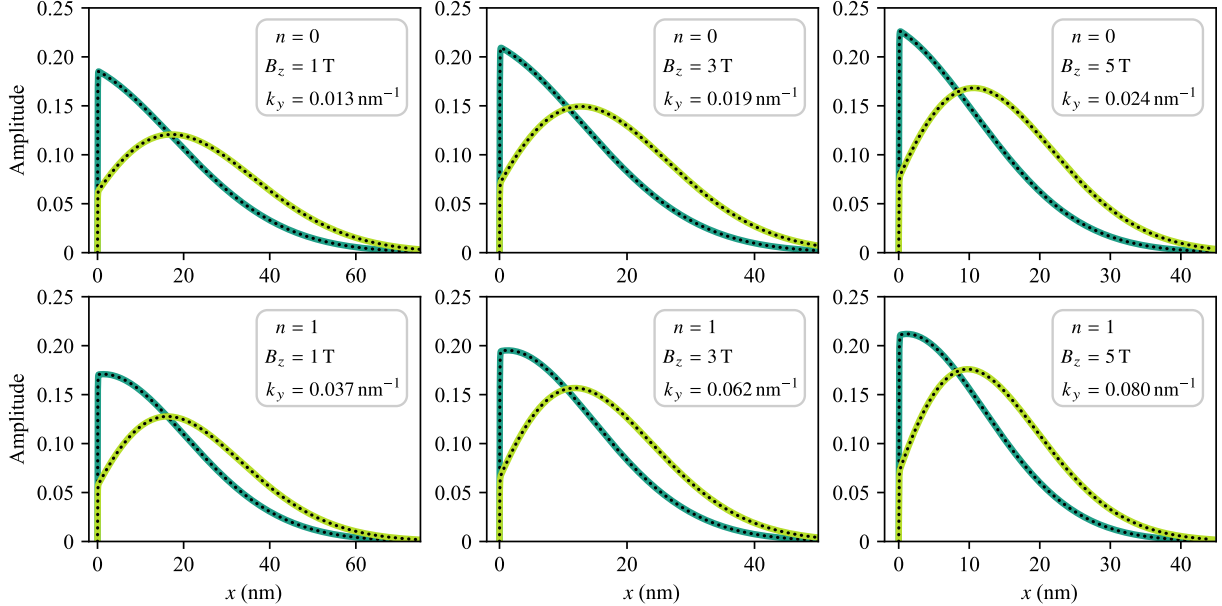


FIG. 7. Wave functions of the edge state of Bi_2Se_3 with $\tau_z = 1$ and several \mathcal{B} and n at the corresponding Landau level energies as calculated by Eq. (9). The full lines are the numerically calculated wave functions, with the dark-green line being the first component and the light-green line the second. The dashed lines are the approximations of Eq. (12), with the k_y corresponding to E_n obtained via the self-consistency relation (C1). It can be seen that the approximation works extremely well at all different values shown.